THE EFFECT OF STEFAN FLOW ON THE MODELS OF DROPLET EVAPORATION

Yigit AKKUS
ASELSAN A.Ş. Haberleşme ve Bilgi Teknolojileri Sektör Bşk., 06200 Yenimahalle, Ankara
yakkus@aselsan.com.tr, ORCID: 0000-0001-8978-3934

Abstract: Droplet evaporation has been widely studied in the literature due to its key role in various applications in science and industry. The problem of droplet evaporation involves various mechanisms in both liquid and vapor phases together with the interface separating them. Modeling of this multiphase problem is not straightforward thereof studied by many researchers but in every time a few different contributing mechanisms could be highlighted. One of the pieces of this puzzle is undoubtedly the Stefan flow, which is always present during the evaporation of a liquid to an insoluble surrounding gas, yet the number of studies exploring its individual contribution to the evaporation remain very restricted. In the current study, the effect of Stefan flow is assessed by employing a recent state-of-the-art model that accounts for all pertinent physics of droplet evaporation. Results reveal that Stefan flow can be responsible for 17% of total evaporation when the droplet is placed on a high temperature substrate. Moreover, it is shown that lower performance of diffusion based models (in gas phase) can be greatly enhanced by incorporating the effect of Stefan flow into the interfacial mass flux equation. In addition, performances of existing *purely diffusion* and *diffusion and Stefan flow* based correlations in the prediction of evaporation rates are elucidated. Last but not least, under varying humidity of the surrounding gas, contribution of individual transport mechanisms in gas phase to the total evaporation rate is found to be unaffected. Based on this result, it is hypothesized that contributions of Stefan flow and natural convection have a linear dependence on the contribution of sole diffusion. The current study clearly demonstrated that Stefan flow considerably enhances the evaporation rate of droplets, especially in the case of high substrate heating. Therefore, future studies on the topic should account for the Stefan flow during the modeling of droplet evaporation.
Keywords: Droplet evaporation, Stefan flow, natural convection, gas diffusion, thermocapillarity, buoyancy.

STEFAN AKIŞININ DAMLACIK BUHARLAŞMA MODELLERİ ÜZERİNDEKİ ETKİSİ

Özet: Bilim ve endüstrideki çeşitli uygulamalarda kilit rolü olması nedeniyle damlacık buharlaşması literatürde yaygın olarak incelenmektedir. Damlacık buharlaşması problemi, sıvı ve buhar fazları ile bu fazları ayıran ara yüzeyde meydana gelen çeşitli mekanizmaları içerir. Modellenmesi kolay olmayan bu çok-fazlı problem birçok araştırmacı tarafından çalışılmıştır, ancak içerdiği mekanizmalardan sadece birkaçı ön plana çıkarılabilmiştir. Bir sıvının o sıvı içerisinde çözünmeyen gaz ortamına buharlaşması sırasında her zaman ortaya çıkan Stefan akışı, bulmacanın parçalarından biridir. Ancak Stefan akışının buharlaşmaya olan katkısını araştıran çalışmaların sayısı oldukça sınırlıdır. Bu çalışmada, Stefan akışının etkisi, tüm ilgili fiziksel mekanizmaları içeren yenilikçi bir model kullanılarak ölçülmüştür. Damlacık yüksek sıcaklıkta bir katı yüzey üzerine yerleştirildiğinde Stefan akışının toplam buharlaşmanın %17'sinden sorumlu olabileceği bu çalışmada gösterilmiştir. Ayrıca, Stefan akışının ara yüzey kütle akısı denklemine dâhil edilmesiyle difüzyon temelli modellerin (gaz fazındaki) düşük performansının büyük ölçüde arttırılabileceği gösterilmiştir. Ayrıca bu çalışmada, sadece difüzyon ile difüzyon ve Stefan akışına dayalı mevcut ilgileşimlerin buharlaşma oranlarını bulma performansları tartışılmıştır. Son olarak, gaz ortamının değişen nem oranları altında, gaz fazındaki münferit taşıma mekanizmalarının toplam buharlaşma hızına olan katkılarında bir değişiklik olmadığı bulunmuştur. Bu sonuca dayanarak, Stefan akışı ve doğal konveksiyonun katkılarının, sadece difüzyonun katkısına doğrusal bir bağımlılığı olduğu düşünülmüştür. Bu çalışma, Stefan akışının, bilhassa ısıtılmış katı yüzeyler üzerinde duran damlacıkların buharlaşma hızlarını kayda değer şekilde arttırdığını göstermiştir. Bu yüzden, bundan sonra yapılacak ilgili damlacık buharlaşması modelleme çalışmaları Stefan akışını da içermelidir.
Anahtar Kelimeler: Damlacık buharlaşması, Stefan akışı, doğal taşınım, gaz difüzyonu, sıcaklığa bağlı değişen kılcallık, kaldırma.

NOMENCLATURE

Symbols

B_M	Spalding mass number
c_p	specific heat capacity [J/kg·K]
c	molar concentration [mol/m^3]

D	binary diffusion coefficient [m^2/s]
$\mathbf{g}$	gravitational acceleration [m/s^2]
h_{fg}	latent heat of evaporation [J/kg]
k	thermal conductivity [W/m·K]
$\dot{m}''_{ev}$	evaporative mass flux [kg/m^2·s]
M	molar mass [kg/mol]

n	unit vector in normal direction
p	pressure [Pa]
R	droplet radius [m]
t	unit vector in tangential direction
T	temperature [ºC]
u	velocity vector [m/s]
Y	mass fraction

Greek Symbols

γ	surface tension [N/m]
ε	emissivity
θ	contact angle [rad]
ρ	density [kg/m^3]
σ	Stefan-Boltzmann constant [W/m$^2 \cdot$K^4]
$\bar{\bar{\tau}}$	stress tensor [Pa]
ϕ	relative humidity

Subscripts

a	air
g	gas
l	liquid
s	droplet surface
surr	surroundings
v	vapor
w	wall
∞	far field

INTRODUCTION

Droplet evaporation is at the center of numerous natural phenomena, scientific processes, and industrial applications including DNA mapping, inkjet printing, and surface coating (Smalyukh *et al.*, 2006; Lim *et al.*, 2009; Wu *et al.*, 2014). In recent years, the interest of thermal scientists in the droplet evaporation has increased because of its potential utilization in electronic cooling applications (Won *et al.*, 2015; Shuai *et al.*, 2018). Evaporating droplets are promising tools in heat removal due to high latent heat of vaporization emerging during phase change. Their utilization in a cooling application can be in different ways. Spray cooling, for instance, uses drying fine droplets, which are continuously generated through a nozzle and thrown to the hot substrate (Kim, 2007). Alternatively, continuously fed constant shape droplets are suggested as an effective cooling solution (Kokalj *et al.*, 2010).

Droplet evaporation is a multi-phase problem combining liquid droplet domain with surrounding gas domain. While the liquid domain consists of a single pure substance, gas domain is the mixture of air and the vapor of the liquid. Therefore, in addition to mass, momentum, and energy balance equations, species transport equation should be considered in the gas domain during the solution. Boundary conditions at the natural boundaries of the problem domain can be easily determined. However, boundary conditions at the droplet surface (*i.e.* at the interface between liquid and gas domains) requires additional attention due to the inherent complexities of coupling of condensed and rarefied phases. Hence, the modeling of droplet evaporation is not straightforward

and is computationally costly. To mitigate the computational challenges, various assumptions have been applied in the modeling of droplet evaporation such as omission of convective transport in liquid and/or gas phases, neglecting Marangoni (thermocapillary) effect and applying Boussinesq approximation to model buoyant flows. Although these simplifications facilitate obtaining a converged solution, they inevitably result in certain errors, the extent of which should be questioned in detail.

Although it was rarely considered in early studies (Duh and Yang, 1989; Lozinski and Matalon, 1993), convective transport inside the droplet is always present and two simultaneous effects trigger it: buoyancy and thermocapillarity. Although the observation of thermocapillary flow in water droplet is controversial in the literature (Ward and Duan, 2004; Xu and Luo, 2007), thermocapillary flow always exists based on the thermophysical properties of pure water as long as there is a temperature gradient at the liquid-vapor interface. Moreover, it was reported that when these both effects are present, thermocapillary flow dictates the internal flow field by dominating the buoyant liquid flow (Bouchenna *et al.*, 2017).

In gas domain, convective transport accompanies the mass diffusion. However, early studies generally followed the semi-empirical correlation of Hu and Larson (2002) as a function of contact angle based on the well-known studies of Deegan *et al.* (1997, 2000). Likewise, many studies considered only the heat and mass diffusion in the gas phase (Girard *et al.*, 2006; Xu *et al.*, 2009). Omission of convection was demonstrated to considerably lower the evaporation rates by the experiments (Kelly-Zion *et al.*, 2011; Carle *et al.*, 2013; Carle *et al.*, 2016). Yet the role of convection has been neglected in almost all numerical studies except a few (Saada *et al.*, 2010; Chen *et al.*, 2017; Pan *et al.*, 2020). It should be noted that natural convection in gas phase becomes stronger with increasing substrate temperatures. Therefore, inclusion of gas flow is critical in the modeling of droplets utilized in the thermal management of high heat flux dissipating electronic components.

Another common assumption in droplet evaporation modeling is the omission of Stefan flow. Except several recent studies (Semenov *et al.*, 2013; Carle *et al.*, 2016; Chen *et al.*, 2017; Pan *et al.*, 2020), evaporation models have neglected the effect of Stefan flow. However, Stefan flow is always present during the evaporation of a liquid to a different surrounding gas, which is insoluble in the liquid. Mechanism of Stefan flow can be understood better by referring to Figure 1. Vapor molecules emitted from the droplet surface diffuse into the air, which is called as vapor diffusion as seen in Figure 1b. Likewise, air molecules diffuse towards to the droplet surface due to the concentration gradient, which is called air diffusion as seen in Figure 1b. However, concentration of air at the droplet surface must vanish since the air is not soluble in the liquid. Therefore, a counter mechanism is necessary to oppose the mass transfer of air towards the interface.

A bulk gas flow, then, originates near the interface and carries the air molecules away from the droplet surface in an equal rate of air diffusion (called air convection in Figure 1b). This flow is called as Stefan flow, and, in addition to the air molecules, it transports the vapor from the interface (called as vapor convection in Figure 1b) as an additional mechanism to the diffusion of vapor. Consequently, when considered in the modeling, Stefan flow results in elevated evaporation rates. Contribution of Stefan flow to the evaporation rates and its effect on the gas flow field were experimentally assessed by several recent studies (Zaitsev *et al.*, 2017; Kabov *et al.*, 2017; Misyura, 2017, 2018). Moreover, empirical model of Carle *et al.* (2016) was utilized to show the effect of Stefan flow on evaporation rates for a certain drop configuration. However, a comprehensive numerical model including all pertinent physics in drop evaporation have not been employed to reveal the explicit contribution of Stefan flow on evaporation rates yet.

Objective of this study is to demonstrate the effect of Stefan flow on droplet evaporation. A recent theoretical framework suggested by Akkus *et al.* (2020) for the modeling of steady droplet evaporation is used to model the evaporation with and without the presence of Stefan flow. In addition to a full-model incorporating all relevant physics in both liquid and gas domain, a model that omits the fluid flow in gas domain (*i.e.* diffusion based model in gas domain) is also applied to assess the effect of Stefan flow on widely used diffusion based models. Moreover, simulations results are compared with the predictions of two well-known correlations: diffusion based correlation of Hu and Larson (2002) and Spalding model (Sazhin, 2005; Carle *et al.*, 2016) accounting for both diffusion and Stefan flow. To the best of author's knowledge, this is the first study assessing the contribution of Stefan flow to the evaporation utilizing a numerical model with temperature dependent thermophysical properties accounting for buoyancy and Marangoni convection in liquid phase together with diffusive and convective transport in gas phase.

THEORETICAL MODELING

In the case of steadily fed droplets, a steady state solution of the governing equations is sought since the geometries of liquid and gas domains do not change with time. A similar approach is also applied for drying droplets due to the fact that the time scale of droplet deformation is significantly longer than mass, momentum or energy transport time scales (Carle *et al.*, 2016; Pan *et al.*, 2020). Consequently, a quasi-steady state solution is applicable for the instantaneous geometry of the droplet and corresponding environment conditions. Almost all of the modeling attempts in previous studies were using the quasi-steady state assumption.

In the present study, steady evaporation from a hemispherical, continuously fed water droplet placed on a heated wall is considered. Surrounding air volume is chosen as much larger than the volume of the droplet to prevent artificial boundary effects. Due to the symmetry, 2-D axisymmetric model is utilized. Figure 2 shows the problem domain together with the boundary conditions. At the far field boundaries, temperature, pressure, and concentration values are set to their ambient values. Symmetry conditions are applied at the droplet axis. Assuming highly conductive substrate material, constant wall temperature is assigned to the substrate surface. Moreover, no slip and no vapor penetration conditions are applied at the substrate surface.

Governing equations are solved in both phases, separately. Conservation equations for mass, linear momentum, and energy are considered in both phases, while species conservation equation for vapor transport is additionally considered in the gas phase. Due to the continuous feeding assumption, droplet shape is preserved during the evaporation, which renders the problem steady state. Steady forms of the governing equations are summarized below:
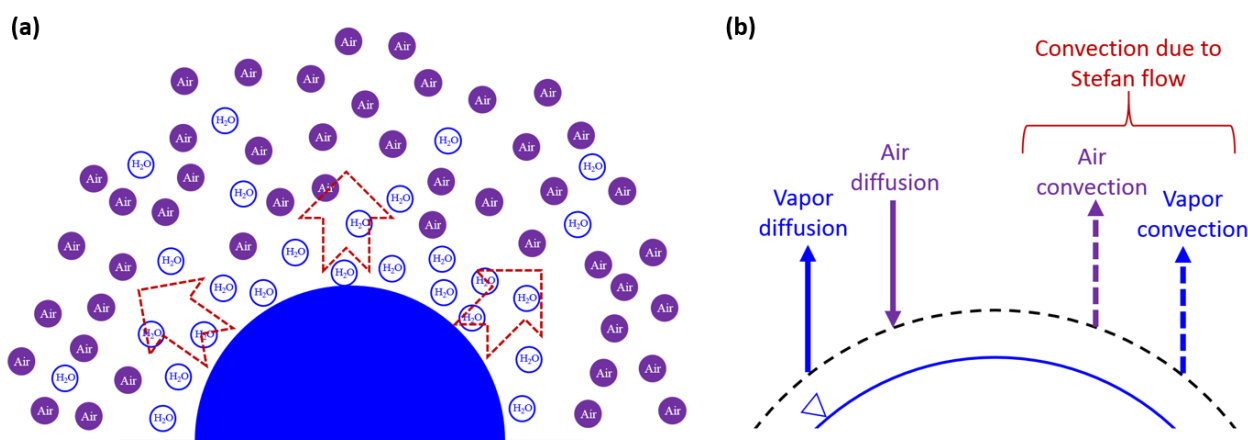

Figure 1. (a) Typical distribution of vapor and air during droplet evaporation. Red arrows show the bulk flow of gas (Stefan flow). (b) Interfacial mass transport mechanisms during droplet evaporation in the vicinity of droplet surface.

$$\nabla \cdot (\rho \boldsymbol{u}) = 0 \tag{1a}$$

$$\rho(\boldsymbol{u} \cdot \nabla)\boldsymbol{u} = -\nabla p + \nabla \cdot \bar{\bar{\tau}} + \rho \boldsymbol{g} \tag{1b}$$

$$\rho c_p \boldsymbol{u} \cdot \nabla T = \nabla \cdot (k \nabla T) + \bar{\bar{\tau}} : \nabla \boldsymbol{u} \tag{1c}$$

$$\boldsymbol{u} \cdot \nabla c_v = \nabla \cdot (D \nabla c_v) \tag{1d}$$

Since droplet and gas domains are solved separately, the interface between liquid and pas phases arises as an additional boundary. Energy, force, and mass balances at this interface should be carefully established. Balance equations, then, serve as boundary conditions for both domains. Energy is transferred from the droplet to the gas phase and surroundings *via* three mechanisms: evaporative heat transfer, conduction, and radiation as shown in Figure 2. Consequently, energy balance reduces to the following equation:

$$\boldsymbol{n} \cdot (-k_l \nabla T_l) = \dot{m}_{ev}'' h_{fg} + \boldsymbol{n} \cdot (-k_g \nabla T_g)$$
$$+ \sigma \varepsilon (T_s^4 - T_{surr}^4) \tag{2}$$
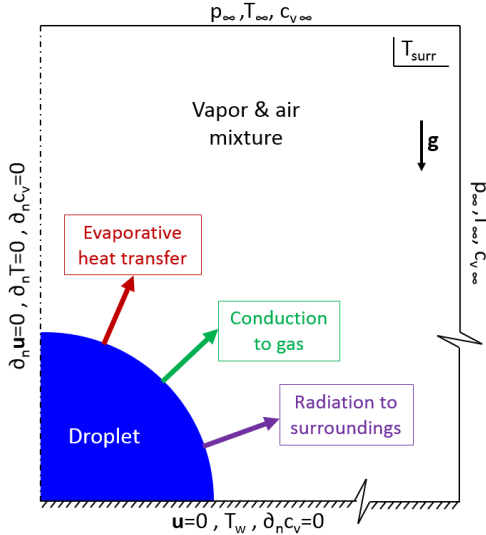

Figure 2. Problem domain and boundary conditions

Majority of interfacial heat transfer is due to the evaporation. Therefore, estimation of evaporative mass flux ($\dot{m}_{ev}''$) is crucial. Contrary to the common approach, diffusion of vapor in the gas phase is not the sole mechanism for the mass transfer. Stefan flow is also responsible for the transport of vapor from the interface. Therefore, evaporative mass flux should be expressed in terms of both transport mechanisms as follows:

$$\dot{m}_{ev}'' = M(-D(\nabla \cdot \boldsymbol{n})c_v + (\boldsymbol{u_g} \cdot \boldsymbol{n})c_v) \tag{3}$$

where $\boldsymbol{u_g}$ is the velocity of the gas flow near the interface. The magnitude of normal gas velocity can be calculated by equating the *air diffusion* (see Fig. 1) towards the interface and *air convection* (see Fig. 1) from the interface as follows:

$$\boldsymbol{u_g} \cdot \boldsymbol{n} = -(D/c_a)(\nabla \cdot \boldsymbol{n})c_a \tag{4}$$

Equation (3) estimates the interfacial mass flux based on the gas phase near the interface. This mass flux must be conserved across the interface. Then normal component of interfacial liquid velocity can be obtained based on the interfacial mass balance as follows:

$$\boldsymbol{u_s} \cdot \boldsymbol{n} = \dot{m}_{ev}'' /\rho \tag{5}$$

Density difference of the phases leads to a jump in normal components of the interfacial velocities. On the other hand, tangential velocities of both phases converge to the same value at the interface. This tangential velocity can be estimated based on the tangential force balance:

$$-\boldsymbol{n} \cdot \bar{\bar{\tau}}_l \cdot \boldsymbol{t} = \nabla \gamma \cdot \boldsymbol{t} \tag{6}$$

In Eq. (6), shear stress associated with the gas phase is omitted. This assumption is justified by a post analysis, which shows that shear of gas is substantially smaller than that of liquid.

Governing equations with the associated boundary conditions are solved using Finite Element Method based solver of COMSOL Multiphysics® software (2018). Embedded grid generator of COMSOL is utilized to create the solution mesh. Liquid-gas interface is divided to equal length arcs before meshing. Grid generation initiates on these arcs and advances towards the liquid and gas domains at a certain growth rate. The number of arcs control the resolution of the solution by determining the density of the resultant mesh at the interface. Grid independence is controlled and secured for every case studied based on the criteria of change of evaporation rate to be less than 0.1%. Coupling of two phases, *i.e.* the application of interfacial boundary conditions to both liquid and gas domains, is not straightforward. Therefore, an iterative solution approach is required to satisfy the interfacial mass, momentum and energy balances (Akkus *et al.,* 2017, 2019). Details of the iterative computational scheme together with the validation of the model were given in the study of Akkus *et al.* (2020), and, therefore, not repeated here.

PREVIOUS CORRELATIONS FOR DROPLET EVAPORATION

Droplet evaporation is commonly present in many applications. Prediction of evaporation rate is of interest in these applications. However, modeling of this complex phenomenon is costly in terms of both computational power and time. Therefore, previously reported correlations are usually utilized to estimate the evaporation rates of droplets in many fields of science and industry. Among these correlations, several influential ones are highlighted in this section.

Deegan *et al.* (1997) explained the coffee ring effect (ring-like deposit along the perimeter of drying coffee droplets) by suggesting the capillary flow (from the center of the droplet towards the edge) as the carrier of colloidal particles when the droplet dries with a pinned contact line (constant contact radius, CCR, mode). They suggested a spatial variation of the evaporation rate

intensifying near the contact line due to the thinning liquid height: $\dot{m}''_{ev} \propto (R - r)^{-\lambda}$. Considering a diffusion limited transport in the gas phase, later, Deegan *et al.* (2000) reported a suitable approximation to the analytical solution of the problem as follows: $\dot{m}''_{ev} \approx J_0[1 - (r/R)^2]^{-\lambda}$, where J_0 was related to vapor mass diffusion and λ was a fitting parameter accounting for the nonuniformity of the evaporation rate along the droplet interface. The relationship between J_0 and λ, and also their dependence to contact angle, θ, were not exactly defined by Deegan *et al.* In a following study, Hu and Larson (2002) provided semi-empirical correlations of $J_0(\theta)$ and $\lambda(\theta)$ as functions of contact angle based on the solution of diffusion equation in the gas phase. After integrating the interfacial mass flux along the droplet surface, Hu and Larson derived a simple correlation for the total evaporation rate from a droplet having a contact angle between 0 and $\pi/2$ as follows:

$$\dot{m}_{ev} = -\pi R D \big(\rho_v|_{T_w} - \rho_v|_{T_\infty}\big)(1.3 + 0.27\theta^2) \qquad (7)$$

Derivation of this correlation was dependent on certain assumptions and conditions. In the gas phase, convective transport (natural convection, Stefan flow etc.) was not accounted for. Moreover, liquid–vapor interface was assumed isothermal. Internal convection inside the liquid was also not considered. Another important aspect was that vapor density in the correlation was suggested to evaluate at substrate (wall) temperature assuming small temperature difference between droplet surface and substrate. Despite these simplifications, correlation of Hu and Larson (2002) was adopted by many subsequent studies because of its simplicity.

Convective mass transfer from droplet surface has been of interest in combustion studies. As a common tool utilized in these studies, Spalding evaporation model (Spalding, 1953) was developed based on the calculation of mass and heat balance separately in each phase at the interface. This model includes the effect of Stefan flow in addition to the diffusive mass transfer, thereby enabling the estimation of evaporation enhancement due to Stefan flow. Sazhin (2005) reported a correlation based on Spalding model assuming vapor and air diffusion coefficients equal:

$$\dot{m}_{ev} = -4\pi R D \big(\rho_v|_{T_\infty} + \rho_a|_{T_\infty}\big)\ln(1 + B_M) \qquad (8a)$$

$$B_M = \big(Y_{v,s} + Y_{v,\infty}\big)/(1 - Y_{v,s}) \qquad (8b)$$

$$Y_{v,s} = \left[1 + \left(\frac{p_\infty}{p_v|_{T_s}} - 1\right)\frac{M_a}{M_v}\right]^{-1} \qquad (8c)$$

During its derivation, Spalding model had also certain assumptions. Firstly, this correlation considers a full spherical droplet. Therefore, its applicability for droplets resting on a substrate with certain contact angle is questionable. Carle *et al.* (2016) speculated that this correlation's functional dependence on geometrical parameters remains the same as for pure diffusive

evaporation. However, in this study, since the geometry of the droplet considered is hemisphere, evaporation rate can be estimated by halving the rate in Eq. (8a) without further modifications to account for the effect of different contact angles. Moreover, Spalding model assumes isothermal droplet and vapor/liquid equilibrium at the interface. During the calculation of vapor pressure near the droplet in Eq. (8c), the isothermal droplet temperature is simply used. However, if the temperature distribution is available for the droplet, temperature of the surface should be considered. In this study, area-weighted average of surface temperature (T_s) is utilized to estimate (saturated) vapor pressure (p_v) near the droplet surface.

RESULTS AND DISCUSSION

Simulations are carried out for a hemispherical water droplet placed on a heated substrate surrounded by ambient air. Size of the droplet and air domains together with the properties of surrounding air are provided in Table 1. Bond number is sufficiently smaller than unity for all cases simulated confirming the spherical shape of the droplet surface. Water surface is assumed to have the emissivity value of 0.97 (Robinson and Davies, 1972). Binary diffusion coefficient of water vapor in air is calculated based on the temperature dependent correlation suggested by Bolz and Tuve (1976). The rest of the thermophysical properties are also considered temperature dependent and evaluated during the simulations utilizing the material library of COMSOL.

Table 1. Geometrical parameters and far field conditions

Droplet radius	2.5 mm
Radius of gas volume	250 mm
Height of gas volume	500 mm
Ambient temperature	30 °C
Ambient pressure	1 atm
Ambient relative humidity	0.25

Considering a solid substrate with sufficiently high thermal conductivity, temperature of the wall is assumed uniform. Substrate temperature is set to 39 °C (Case-1) and 74 °C (Case-2) matching those of a previous study (Akkus *et al.,* 2019, 2020), where it was demonstrated that the increase of substrate temperature has paramount effect on the evaporation rate and the physics of the fluids in both phases. Thermocapillary (Marangoni) flow is triggered by the variation of surface tension with changing temperature. The presence of Marangoni flow for water is contentious in the literature (Ward and Duan, 2004; Xu and Luo, 2007). Theoretically, Marangoni flow must be present in evaporating droplets with considerable surface temperature variation. However, common belief for vanishing Marangoni flow in many droplet experiments is the high attraction of water molecules to the surfactants (Savino *et al.*, 2003). Consequently,
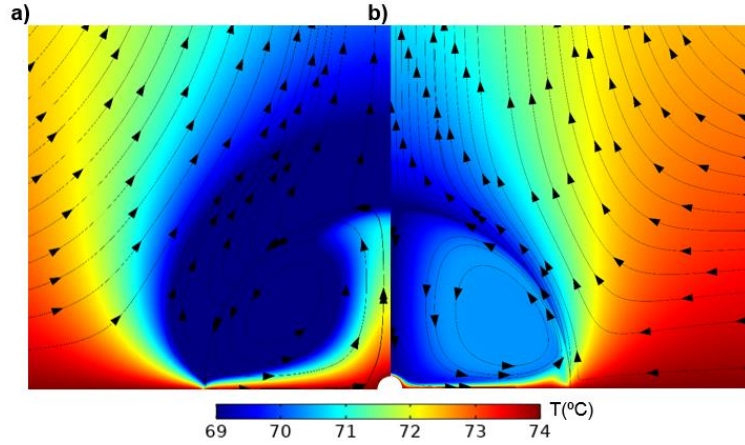
Figure 3. Temperature field and streamlines by **FM** in droplet and gas region near the droplet surface for Case-2 **a)** without and **b)** with thermocapillary flow.

Marangoni flow is not always observable and, in its absence, buoyancy drives the internal liquid flow inside the droplets (Ruiz and Black, 2002; Lu *et al.*, 2011; Bouchenna *et al.*, 2017; Akkus *et al.*, 2019). In this study, simulations are carried out with and without the presence of Marangoni flow to demonstrate the effect of Stefan flow on evaporation rates and dynamics for both cases.

First, simulations are carried out considering all relevant physics including Stefan flow. These simulations are named as full model (called **FM** hereafter). The temperature distribution inside the droplet and the gas region near the droplet is shown in Figure 3, where only the results of Case-2 are provided since temperature and flow patterns are similar in both cases. When Marangoni flow is absent, buoyant flow carries the liquid from substrate to the apex along the centerline. Liquid, then, cools due to evaporation and moves along the droplet surface towards the contact line. The resultant flow pattern forms a vortex as shown in Fig. 3a. When Marangoni (thermocapillary) flow is accounted for, flow pattern is also a vortex but in the reverse direction (see Fig. 3b). In this case, liquid is transported along the droplet surface towards the apex due to the increasing

surface tension. This thermocapillary flow is much stronger than buoyant flow and carries much more energy from the hot wall to the droplet. Consequently, temperature rise is higher in the droplet and at the droplet surface when Marangoni flow is present.

After **FM** simulations, Stefan flow is canceled by setting the normal component of the gas velocity at the interface (*i.e.* $u_g \cdot n = 0$). Simulations of full model without Stefan flow is named as **FM-S**. Resultant velocity magnitude fields and superimposed streamlines in droplet and gas region near the droplet surface without Marangoni flow for Case-2 are shown in Figure 4a. To enable a direct comparison, predictions of **FM**, which includes Stefan flow, are also provided in Figure 4b. It should be noted that strong thermocapillary flow (in tangential direction) dominates the Stefan flow (in radial direction) leading to an overall tangential flow in the close vicinity of the droplet surface (see Figure 3b). Therefore, changes in the magnitude of Stefan flow are not noticeable in the presence of thermocapillarity, which constitutes the reason of reporting the results in Figure 4 for only buoyancy driven internal flow cases. Figure 4 clearly demonstrates that velocity field and magnitudes
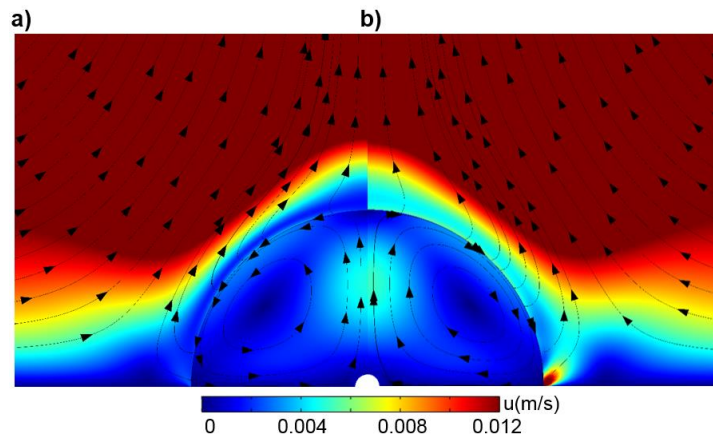

Figure 4. Velocity magnitude field and streamlines in droplet and gas region near the droplet surface without Marangoni flow for Case-2 **a)** without (**FM-S**) and **b)** with (**FM**) Stefan flow.

314

Table 2. Evaporation rate (in μg/s) estimation of different models. Percentage values in parenthesis reflect the ratio of the evaporation rate estimation of a model to that of **FM**.

	w/o Marangoni		w/ Marangoni	
	Case-1	**Case-2**	**Case-1**	**Case-2**
Diffusion model (**DM**)	15.0 (77%)	87.2 (64%)	16.8 (69%)	108.6 (46%)
Diffusion model w/ Stefan flow (**DM+S**)	15.9 (82%)	113.3 (84%)	17.9 (73%)	159.3 (67%)
Diffusion based correlation: Hu&Larson (2002) (**HL**)	17.4 (90%)	114.1 (84%)	17.4 (71%)	114.1 (48%)
Diffusion&Stefan flow based Spalding correlation (**SP**)	15.9 (82%)	105.4 (78%)	18.4 (75%)	142.8 (60%)
Full model w/o Stefan flow (**FM-S**)	18.6 (96%)	116.7 (86%)	23.2 (95%)	197.5 (83%)
Full model (**FM**)	19.4 (100%)	135.4 (100%)	24.5 (100%)	238.4 (100%)

are greatly affected depending on the presence of Stefan flow. In its absence, velocity magnitudes are lower in the close vicinity of the interface. Moreover, gas flow originating from the droplet surface immediately bends in upward direction. In the presence of Stefan flow, normal gas flow originating from the interface is stronger. Due to the strong evaporation near the contact line, a gas flow jet emerges in the normal direction near the contact line in accordance with previous studies (Carle *et al.*, 2016; Pan *et al.*, 2020), which is not apparent in the results of **FM-S** in Figure 4a.

Many studies in the literature have considered only the diffusion of heat and vapor in gas phase because of its relatively low computational cost. These diffusion based models can be useful as long as the convective transport is weak in the gas phase (slight substrate heating etc.). A diffusion limited model (**DM** hereafter) can be constructed by canceling the gas flow in **FM**. Although gas flow is not present in **DM**, the effect of the absence of Stefan flow on evaporation rates can be assessed by including the convection component of mass flux in Eq. (3) since the estimation of normal velocity at the interface is dependent on the concentration distribution of air solely (see Eq. (4)). Therefore, this study also simulates a diffusion limited evaporation with the added effect of mass transfer associated with the Stefan flow. This model is called as **DM+S**. Resultant evaporation rates of all models simulated together with the predictions of diffusion based correlation of Hu and Larson (2002) (**HL** hereafter) and Spalding model (**SP** hereafter) are summarized in Table 2.

Results demonstrate that the rise in the substrate temperature and the presence of Marangoni flow enhance the evaporation rates, as expected. Omission of Stefan flow in modeling result in the underestimation of evaporation rates by 4–17%. Underestimation of **FM-S** substantially increases with increasing substrate temperature. In fact, superheat value of 9 °C (Case-1) results in the underestimation evaporation rates by only 4–5%. This result is in conjunction with the study of Semenov *et al.* (2013), where Stefan flow was reported to be negligible in the case of evaporation from droplets resting on non-heated high conductive substrates. Moreover, results exhibit that the effect of Stefan flow on

evaporation is slightly affected by the presence of thermocapillary flow.

Diffusion limited evaporation approach is expected to fail in the presence of strong natural convection of gas phase, which occurs in the case of substrates with elevated temperatures. For instance, in this study, **DM** underestimates evaporation rate by 54% in the case of high substrate temperature (with Marangoni flow); however, this failure can be greatly compensated by the inclusion of the mass flow associated with Stefan flow. For the same case, utilization of **DM+S** enhances the evaporation rate by 47%. In the absence of Marangoni flow, **DM+S** still enhances the evaporation rate greatly (by 30%). In the case of low substrate temperature, on the other hand, enhancement of evaporation rates by **DM+S** remains restricted (6–7%).

While **HL** considers the diffusion of heat and vapor in gas phase solely, **SP** additionally accounts for the Stefan flow, which is, in fact, expected to increase the evaporation rate prediction of **SP**. Yet, in the absence of Marangoni flow, **HL** predicts higher evaporation rates than **SP**. This surprising result is understandable when the temperature selection in the evaluation of vapor properties near the droplet surface is revisited. **HL** utilizes substrate temperature in the estimation of vapor density near the interface in Eq. (7), whilst **SP** considers the surface temperature of the droplet in the calculation of vapor pressure near the interface. In the case of a buoyancy driven internal flow, interface temperature becomes cooler than that of a droplet with Marangoni flow (Lu *et al.*, 2011; Akkus *et al.*, 2019). Therefore, the difference between substrate temperature and average interface temperature is higher in droplets with a buoyancy driven internal flow. Consequently, the vapor pressure near the surface, thereby the evaporation rate, is underestimated by **SP** compared to **HL** in the absence of Marangoni flow. However, when thermocapillarity is present, enhanced heat transfer from the substrate to the interface due to strong Marangoni flow increases the interface temperature, which increases the evaporation rate prediction of **SP**. In addition, in this study, comparisons of the effect of Stefan flow using full and diffusion limited models exhibit that contribution of Stefan flow to the evaporation rates is higher in the presence of Marangoni flow. Thus, **SP** predicts higher

Table 3. Evaporation rate (in μg/s) estimation of different models for Case-2 across different relative humidity values of ambient air. Percentage values in parenthesis reflect the ratio of the evaporation rate estimation of a model to that of **FM**.

	w/o Marangoni			w/ Marangoni		
	ϕ=1	ϕ=0.25	ϕ=0	ϕ=1	ϕ=0.25	ϕ=0
DM	77.8 (65%)	87.2 (64%)	90.2 (65%)	96.4 (46%)	108.6 (46%)	111.2 (45%)
DM+S	102.2 (85%)	113.3 (84%)	117.4 (84%)	142.4 (67%)	159.3 (67%)	163.7 (66%)
HL	102.6 (86%)	114.1 (84%)	118.0 (85%)	102.6 (49%)	114.1 (48%)	118.0 (48%)
SP	101.0 (84%)	105.4 (78%)	106.6 (77%)	136.9 (65%)	142.8 (60%)	144.7 (59%)
FM-S	102.6 (86%)	116.7 (86%)	121.4 (87%)	171.4 (81%)	197.5 (83%)	206.5 (84%)
FM	120.0 (100%)	135.4 (100%)	139.0 (100%)	211.3 (100%)	238.4 (100%)	247.3 (100%)

evaporation rates than **HL** when Marangoni flow is present. Specifically, in the case of hot substrate, choice of **SP** instead of **HL** improves the evaporation rate by 25%.

Additional simulations are carried out under extreme humidity conditions: dry (ϕ=0) and saturated (ϕ=1) air. Since the deviations resulting from simplifying assumptions become larger with increasing substrate temperature, only Case-2 is considered. Results of these simulations together with the corresponding results of previous (ϕ=0.25) simulations are provided in Table 3 to demonstrate the tendency of evaporation rates across ambient air with varying humidity. Results exhibit that increasing vapor fraction in ambient gas reduces the evaporation rate, whilst Marangoni flow inside the droplet enhances the evaporation, as expected. Moreover, evaporation rate prediction of **HL** exceeds that of **SP** in the absence of Marangoni flow due to the lower surface temperature of the droplet in this case as explained previously. Another observation is the restricted increase (15–17%) of evaporation rates between dry and saturated ambient air cases. However, this result can be attributed to the selection of ambient temperature (30 °C), at which the increase in vapor density difference between droplet surface and far field (*i.e.* $\rho_v|_{T_s} - \rho_v|_{T_\infty}$) from saturated to dry air cases is approximately 15%.

On the other hand, results in Table 3 manifest that at a given substrate and ambient temperature, contribution of individual transport mechanisms in gas phase (diffusion, Stefan flow, and natural convection) to the total evaporation rate is unaffected by humidity of the air. In other words, vapor mass transfer rates associated with diffusion, Stefan flow, and natural convection increase linearly with increasing density difference of vapor between near droplet and far field regions. It should be noted that **HL**, as a diffusion limited correlation, relies on the density difference (see Eq. (7)). In this perspective, the density difference can be viewed as a measure of the diffusion component of the total evaporation. Therefore, current results may suggest that contributions of Stefan flow and natural convection scale is linearly dependent on the rate of diffusion. Linear dependence of Stefan flow and diffusion limited evaporation was also suggested by

Semenov *et al.* (2013). In addition, linear dependence of natural convection and diffusion limited evaporation can be inferred from the empirical correlation of Carle *et al.* (2016), where the term representing the diffusion limited evaporation multiplies the other terms in the correlation.

CONCLUSION

An innovative model of droplet evaporation is utilized to evaluate the effects of transport mechanisms, specifically the Stefan flow, on the evaporation rates. Steady evaporation from a hemispherical water droplet placed on a heated flat substrate is considered. Simulations are carried out across varying substrate temperatures and humidity values of surrounding air. Different scenarios based on the presence of thermocapillary convection are also simulated. Results exhibit that omission of Stefan flow leads to the considerable underestimation of evaporation rates (up to 17%) for high substrate temperatures cases, while its effect is very restricted in near isothermal evaporation cases. Inclusion of the mass transfer associated with the Stefan flow is demonstrated to result in a great compensation of the deficit of total evaporation rate in diffusion limited (in gas phase) models. Therefore, despite the exclusion of gas flow, diffusion based models can still account for the effect of Stefan flow. In the absence of Marangoni flow, existing correlations of droplet evaporation (**HL** and **SP**) underestimate the evaporation rate by 10–23%. However, they severely underestimate evaporation rate in the presence of Marangoni flow (25–52%), yet the predictions of **SP** are better than **HL** since it accounts for the Stefan flow. Under varying humidity of the air, contribution of individual transport mechanisms in gas phase to the total evaporation rate is found to be unchanging, which suggests the linear dependence of not only diffusion but also Stefan flow and natural convection on the density difference of vapor between droplet surface and ambient air.

REFERENCES

Akkuş Y., Cetin B. and Dursunkaya Z., 2017, Modeling of Evaporation from a Sessile Constant Shape Droplet. In *ASME 2017 15th International Conference on Nanochannels, Microchannels, and Minichannels*. American Society of Mechanical Engineers Digital Collection.

Akkus Y., Çetin B. and Dursunkaya Z., 2019, An Iterative Solution Approach to Coupled Heat and Mass Transfer in a Steadily Fed Evaporating Water Droplet, *J. Heat Transf.*, 141, 031501.

Akkus Y., Çetin B. and Dursunkaya Z., 2020, A Theoretical Framework for Comprehensive Modeling of Steadily Fed Evaporating Droplets and the Validity of Common Assumptions, *Int. J. Therm. Sci.*, 158, 106529.

Bolz R. and Tuve G., 1976, Handbook of Tables for Applied Engineering Science, CRC Press, Cleveland, 2nd edition.

Bouchenna C., Saada M. A., Chikh S. and Tadrist L., 2017, Generalized Formulation for Evaporation Rate and Flow Pattern Prediction Inside an Evaporating Pinned Sessile Drop, *Int. J. Heat Mass Tran.*, 109, 482-500.

Carle F., Sobac B. and Brutin D., 2013, Experimental Evidence of the Atmospheric Convective Transport Contribution to Sessile Droplet Evaporation, *Appl. Phys. Lett.*, 102, 061603.

Carle F., Semenov S., Medale M. and Brutin D., 2016, Contribution of Convective Transport to Evaporation of Sessile Droplets: Empirical Model, *Int. J. Therm. Sci.*, 101, 35-47.

Chen Y. H., Hu W. N., Wang J., Hong F. J. and Cheng P., 2017, Transient Effects and Mass Convection in Sessile Droplet Evaporation: The Role of Liquid and Substrate Thermophysical Properties, *Int. J. Heat Mass Tran.*, 108, 2072-2087.

COMSOL Multiphysics® v. 5.4. www.comsol.com. COMSOL AB, Stockholm, Sweden, 2018.

Deegan R. D., Bakajin O., Dupont T. F., Huber G., Nagel S. R. and Witten, T. A., 1997, Capillary Flow as the Cause of Ring Stains From Dried Liquid Drops, *Nature*, 389, 827-829.

Deegan R. D., Bakajin O., Dupont T. F., Huber G., Nagel S. R. and Witten T. A., 2000, Contact Line Deposits in an Evaporating Drop, *Phys. Rev. E*, 62, 756.

Duh J. C. and Yang W. J., 1989, Numerical Analysis of Natural Convection in Liquid Droplets by Phase Change, *Numer. Heat Transfer*, 16, 129-154.

Girard F., Antoni M., Faure S. and Steinchen A., 2006, Evaporation and Marangoni Driven Convection in Small Heated Water Droplets, *Langmuir*, 22, 11085–11091.

Hu H. and Larson R. G., 2002, Evaporation of a Sessile Droplet on a Substrate, *J. Phys. Chem. B*, 106, 1334-1344.

Kabov O. A., Zaitsev D. V., Kirichenko D. P. and Ajaev V. S., 2017, Interaction of Levitating Microdroplets with Moist Air Flow in the Contact Line Region, *Nanosc. Microsc. Therm. Eng.*, 21, 60-69.

Kelly-Zion P. L., Pursell C. J., Vaidya S. and Batra J., 2011, Evaporation of Sessile Drops under Combined Diffusion and Natural Convection, *Colloid. Surface. A*, 381, 31-36.

Kim J., 2007, Spray Cooling Heat Transfer: The State of the Art, *Int. J. Heat Fluid Flow*, 28, 753-767.

Kokalj T., Cho H., Jenko M. and Lee L. P., 2010, Biologically Inspired Porous Cooling Membrane Using Arrayed-droplets Evaporation, *Appl. Phys. Lett.*, 96, 163703.

Lim T., Jeong J., Chung J. and Chung J. T., 2009, Evaporation of Inkjet Printed Pico-liter Droplet on Heated Substrates with Different Thermal Conductivity, *J. Mech. Sci. Technol.*, 23, 1788-1794.

Lozinski D. and Matalon M., 1993, Thermocapillary Motion in a Spinning Vaporizing Droplet, *Phys. Fluids A Fluid*, 5, 1596-1601.

Lu G., Duan Y. Y., Wang X. D. and Lee, D. J., 2011, Internal Flow in Evaporating Droplet on Heated Solid Surface, *Int. J. Heat Mass Tran.*, 54, 4437-4447.

Misyura S. Y., 2017, Evaporation of a Sessile Water Drop and a Drop of Aqueous Salt Solution, *Sci. Rep.*, 7, 1-11.

Misyura S. Y., 2018, Non-isothermal Evaporation in a Sessile Droplet of Water-salt Solution, *Int. J. Therm. Sci.*, 124, 76-84.

Robinson P. J. and Davies J. A, 1972, Laboratory Determinations of Water Surface Emissivity, *J. Appl. Meteor.*, 11, 1391-1393.

Ruiz O. E. and Black W. Z., 2002, Evaporation of Water Droplets Placed on a Heated Horizontal Surface, *ASME J. Heat Transf.*, 124, 854–863.

Pan Z., Weibel J. A. and Garimella S. V., 2020, Transport Mechanisms during Water Droplet Evaporation on Heated Substrates of Different Wettability, *Int. J. Heat Mass Tran.*, 152, 119524.

Saada M. A., Salah C. and Lounes T., 2010, Numerical Investigation of Heat and Mass Transfer of an

Evaporating Sessile Drop on a Horizontal Surface, *Phys. Fluids*, 22, 112115.

Savino R., Paterna D. and Lappa M., 2003, Marangoni Flotation of Liquid Droplets, *J. Fluid Mech.*, 479, 307–326.

Sazhin S., 2005, Modelling of Heating, Evaporation and Ignition of Fuel Droplets: Combined Analytical, Asymptotic and Numerical Analysis. In *Journal of Physics: Conference Series*, 22, 174.

Semenov S., Starov V. M. and Rubio R. G., 2013, Evaporation of Pinned Sessile Microdroplets of Water on a Highly Heat-conductive Substrate: Computer Simulations, *Eur. Phys. J-Spec Top.*, 219, 143-154.

Shuai S., Du Z., Ma B., Shan L., Dogruoz B. and Agonafer D., 2018, Numerical Investigation of Shape Effect on Microdroplet Evaporation, ASME 2018 International Technical Conference and Exhibition on Packaging and Integration of Electronic and Photonic Microsystems, American Society of Mechanical Engineers, V001T04A010.

Smalyukh I. I., Zribi O. V., Butler J. C., Lavrentovich O. D. and Wong G. C. L., 2006, Structure and Dynamics of Liquid Crystalline Pattern Formation in Drying Droplets of DNA, *Phys. Rev. Lett.*, 96, 177801.

Spalding D. B., 1953, The Combustion of Liquid Fuel, Pittsburgh.

Ward C. and Duan F., 2004, Turbulent Transition of Thermocapillary Flow Induced by Water Evaporation, *Phys. Rev. E,* 69, 056308.

Won Y., Cho J., Agonafer D., Asheghi M., and Goodson K.E., 2015, Fundamental Cooling Limits for High Power Density Gallium Nitride Electronics, IEEE Trans. *Compon. Packag. Manuf. Technol.*, 5, 737-744.

Wu H., Chen L. X., Zeng X. Q., Ren T. H. and Briscoe, W. H., 2014, Self-assembly in an Evaporating Nanofluid Droplet: Rapid Transformation of Nanorods into 3D Fibre Network Structures, *Soft Matter*, 10, 5243-5248.

Xu X. and Luo J., 2007, Marangoni Flow in an Evaporating Water Droplet, *Appl. Phys. Lett.*, 91, 124102.

Xu X., Luo J. and Guo D., 2009, Criterion for Reversal of Thermal Marangoni Flow in Drying Drops, *Langmuir*, 26, 1918-1922.

Zaitsev D. V., Kirichenko D. P., Ajaev V. S. and Kabov O. A., 2017, Levitation and Self-organization of Liquid Microdroplets over Dry Heated Substrates, *Phys. Rev. Lett.*, 119, 094503.

Yiğit AKKUŞ is a senior engineer in ASELSAN A.Ş. He received his B.Sc. and minor degrees from the Mechanical Engineering and Materials and Metallurgical Engineering Departments of Middle East Technical University, Ankara, Turkey, in 2009, respectively. He obtained his Ph.D. degree from the Mechanical Engineering Department of Middle East Technical University in 2015. He was a post-doctoral fellow in Mechanical Engineering Department of Southern Methodist University, Dallas, U.S.A., in 2017-2018. Dr. Akkuş is responsible for the thermal management and packaging of high heat flux electronics in ASELSAN. His research focuses on macro-, micro- and nano-scale heat transfer, two-phase passive heat spreaders, thin film evaporation and condensation, droplet evaporation and molecular dynamics simulations. He currently teaches "AAR-652 Passive Heat Exchange Devices and Phase Change" course in ASELSAN Academy.